Nanocomposite nc-TiC/*a*-C thin films for electrical contact applications

Erik Lewin,[a] Ola Wilhelmsson, and Ulf Jansson
Department of Materials Chemistry, The Ångström Laboratory, Uppsala University, P.O. Box 538, SE-751 21 Uppsala, Sweden

(Received 31 March 2006; accepted 17 July 2006; published online 1 September 2006)

Thin film nanocomposites of nanocrystalline TiC embedded in a matrix of amorphous carbon have been prepared by nonreactive unbalanced dc-magnetron sputtering. These samples have been tested as coating materials for electrical contacts and show great potential as an alternative to traditional metallic coatings for contacts subjected to wear and friction. Through variation of composition and deposition temperature different microstructures have been attained. The coatings have been characterized using x-ray diffraction, x-ray photoelectron spectroscopy, and Raman spectroscopy. The performance of the coatings has been coupled to the microstructure whereby tuning and optimization possibilities have been identified. © *2006 American Institute of Physics*.
[DOI: 10.1063/1.2336302]

INTRODUCTION

Electrical contacts are often subjected to a wide variety of stresses such as corrosion, wear, and fretting, leading to decreased performance and a shortened life span of the components. Traditionally contact elements are coated with a reasonably noble metal. In nonstationary (i.e., sliding or switching) contact arrangements these soft metallic coatings tend to smear, giving rise to high friction and abrasive wear of the material, thus increasing the risk of component failure and shortening its life span. Hence there is a need for other types of contact coatings that have low friction and wear, coupled with electrical performance that matches traditional metallic coatings.

Well-known wear-resistant and electrically conductive ceramic thin film materials, such as metal carbides, are generally too hard and brittle to be used as coatings on electrical contacts. The bulk of an electrical contact is usually made from a highly conductive and reasonably inexpensive metal, when two such contact members (with or without a traditional metal coating) make contact they deform, increasing the number of contact spots and their area (and hence true area of contact). The largest contribution to the contact resistance comes from the restriction of the current flux through the contact spots.[1–4] A coating consisting of pure metal carbide would not allow a deformation as described above, leading to a much smaller area of true contact, and hence an unacceptably high contact resistance, even though the coating itself has a reasonably high electrical conductivity.

A potential class of materials previously not used for contacts is nanocomposites, where an appropriate combination of electrical and mechanical properties may be achieved by nanoscale combination of two or more phases. A combination of small, hard and highly conductive metal carbide particles, embedded in a matrix of a softer, and reasonably conductive amorphous carbon phase represents one possible solution. The carbide particles give mechanical stability, hardness, and stand for the major electrical conduction of the film. The matrix phase allows the material to deform to increase the true contact area, giving an acceptable contact resistance, and gives low friction. These types of coating systems have to a very limited extent been studied as possible contact materials, even when mechanical, tribological, and electrical properties[5–13] indicate that they are good candidates. Some work on electrical contact properties have been done on nanocomposite coatings where TiC particles are embedded in an amorphous SiC matrix.[14]

In the present work we have studied thin films of nanocrystalline TiC (nc-TiC) in an amorphous carbon (*a*-C) matrix. Coatings of nc-TiC/*a*-C films have previously received quite a lot attention (see, for example, Refs. 7, 8, 10, and 15–18) but not as electrical contact material. In many contact applications the bulk of the contact member is made from metals with relatively low melting points. Hence deposition temperatures are preferably kept as low as possible. We have synthesized coatings by nonreactive magnetron sputtering. To investigate the effect of deposition temperature on the film microstructure we have deposited films from room temperature up to 400 °C. Furthermore the composition of the films has been varied. These coatings have been characterized with respect to phase and microstructure, as well as with respect to electrical properties, and also to some extent mechanical properties. The variation in deposition parameters (composition and deposition temperature) will enable us to seek relations between synthesis conditions and the phase and microstructure (i.e., controlling the phase and microstructure), as well as relations between microstructure and the properties (i.e., understanding the properties).

EXPERIMENT

Deposition was carried out in an ultrahigh vacuum chamber (base pressure of 10^{-10} Torr) by nonreactive, unbalanced dc-magnetron sputtering from separate 2 in. elemental targets, supplied by Kurt J. Lesker Company Ltd. (purity specified as 99.995% and 99.999% for Ti and C, respectively). Sputter deposition rates of respective element were controlled by regulation of the magnetron currents. Through

[a]Electronic mail: erik.lewin@mkem.uu.se

tuning of magnetron currents samples with carbon contents between 46 and 88 at. % were deposited. Sample thickness was kept constant at about 0.2 μm. The Ar plasma was generated at a constant pressure of 3.0 mTorr, with a flow rate of Ar into the chamber of 150 SCCM (SCCM denotes cubic centimeter per minute at STP). Substrates were placed about 15 cm below the magnetrons on a rotating substrate holder. Deposition was carried out simultaneously on single crystal α-$Al_2O_3(00\ell)$ substrates (12.5×12.5 mm^2) and on Ni- and Pd-plated Al washers (10×10 mm^2), simulating an application specific contact member. Films deposited on Al_2O_3 substrates were used for composition and phase analysis, while the films deposited Al washers were primarily used for determination of contact resistance. One sample was also deposited on powder metalurgical steel for tribological and mechanical evaluations. Substrates were heated by a BN plate with W wires, situated about 5 mm below the substrates. The substrate temperature was varied from room temperature (unheated) to 400 °C. The temperature was monitored using a Mikron M90-0 infrared pyrometer, calibrated against a TiC thin film using a thermoelement. Prior to deposition substrates were preheated for at least 30 min, and targets were presputtered for at least 10 min.

The principal methods of film characterization were x-ray photoelectron spectroscopy (XPS) [also known as electron spectroscopy for chemical analysis (ESCA)] for compositional analysis and x-ray diffraction (XRD) for structural analysis. XPS was carried out on a Physical Systems Quantum 2000 spectrometer using monochromatic Al $K\alpha$ radiation. Sensitivity factors were determined for reference samples of binary compounds with known composition; energy calibration was made with Au and Ag reference samples. For all films, depth profiles were acquired by rastered Ar^+-ion sputtering over an area of 1×1 mm^2 with ions having an energy of 2 keV. The XPS analysis area was set to a diameter of 100 μm. High-resolution XPS spectra of the C1*s* peak were recorded after Ar^+-ion sputtering. XRD measurements were carried out on a Philips X'pert diffractometer. For grazing incidence (GI) and θ-2θ scans, parallel beam geometry was used. All XRD measurements were performed using Cu $K\alpha$ radiation. All presented diffractograms have been background corrected. Selected samples were also analyzed by Raman spectroscopy, using a Renishaw micro-Raman system 2000 with an excitation wavelength of 514 nm. Additional morphological information was also given by atomic force microscopy (AFM) and scanning electron microscopy (SEM) imaging using TopoMetrix TMX2000 and Leo 1550 FEG microscopes.

Resistivities of the films were determined by four-point probe measurements on the samples deposited on the insulating Al_2O_3 substrates using equipment from Jadel Engineering Ltd. The contact resistance of samples deposited on washers was measured using custom-designed equipment at Impact Coatings in Linköping, Sweden, which allowed the voltage drop over the contact interface to be measured as a function of contact force. All measurements were made against a Ag-coated countercontact. In the contact resistance measurements the nominal contact area was 1 cm^2.

Mechanical properties were evaluated with a Nanoindenter XP, using a Berkovich diamond tip, a penetration depth of 100 nm, and a matrix of 4×5 indents. Hardness and elastic modulus were calculated according to method described by Oliver and Pharr.[19] The coefficient of friction was measured with a pin-on-disktribometer with a constant gliding speed of 0.1 m/s and a gliding radius of 2.5 mm. The normal contact force was 5 N, and the ball diameter was 6 mm. No lubrication was used and test was performed at ambient environment with ball-bearing steel as countersurface.

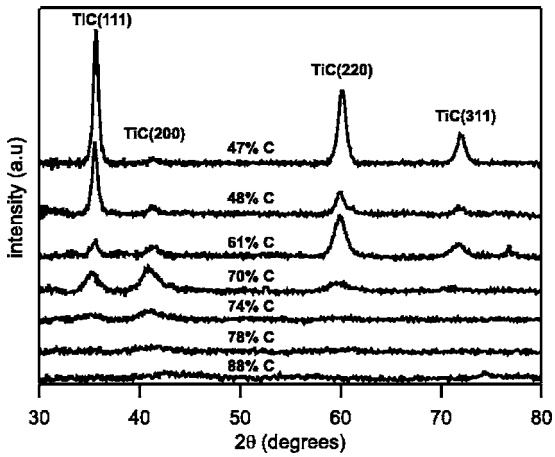

FIG. 1. Diffractograms from GI scans recorded for samples of different compositions deposited at 300 °C on Al_2O_3 substrates.

RESULTS

Characterization of nc-TiC/*a*-C films

XRD

Figure 1 shows a series of diffractograms recorded for nc-TiC/*a*-C films with different compositions. All films were deposited on Al_2O_3 substrates. This substrate was more suitable for film characterization than the contact substrate (partly due to peak overlap and surface roughness). As will be seen below, however, similar results are attained for both substrates. The diffractograms are recorded by GI scans, which increases the signal from the film relative to the substrate, and in the case of a single crystal substrate usually leads to a complete cancellation of the substrate peaks. All observed peaks in Fig. 1 can be indexed to TiC_x,[20] and it is clear that samples with a carbon content higher than 75 at. % are x-ray amorphous. Furthermore, the presence of several different crystal orientations clearly shows the polycrystalline structure of the observed TiC_x. The cell parameter of the TiC_x is found to vary between 4.36 and 4.41 Å, which is larger than literature values for bulk samples of comparable carbon content.[21] In Fig. 2 three typical diffractograms for nc-TiC/*a*-C films deposited on contact substrates are shown together with that of a blank contact substrate. Consistent with the results above all nonsubstrate peaks can be indexed as TiC_x. Hence there are no indications of any interface phases between the contact substrate and the growing film. Trends in cell parameter and peak broadening are also similar to those observed from diffractograms in Fig. 1, the latter will be discussed below. Since films deposited on metallic

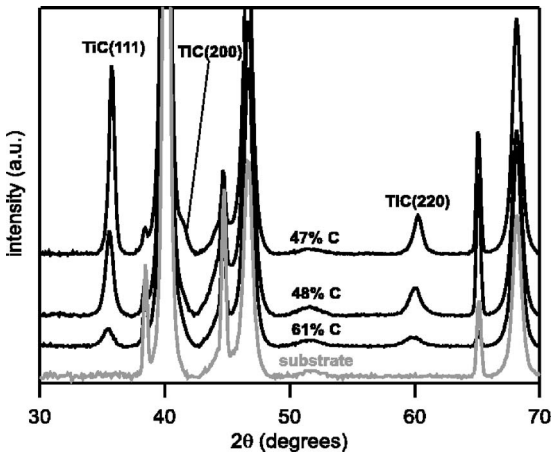

FIG. 2. Diffractograms from GI scans of coatings with different compositions deposited on contact material substrates. The gray diffractogram is a reference from a blank substrate.

contact substrates and on inert Al_2O_3 substrates are the same we will base our analysis on the samples deposited on Al_2O_3 substrates. In Fig. 3 diffractograms recorded from samples deposited at different temperatures are presented. These samples all have carbon contents of 51–55 at. %. As with the series with varying carbon contents all peaks in Fig. 3 can be indexed as TiC_x.[20] The relative intensity of the (200) and (311) peaks changes with increased deposition temperature and can be contributed to a change in the texture of the films. From the XRD results we conclude that nc-TiC_x is present in samples with a carbon content lower than 75 at. %.

As can be seen from the GI diffractogram in Fig. 1, the intensity of the peaks (indicating amount of crystalline phase) is reduced, and the peak broadening (indicating crystallite size and/or intrinsic stress) increases with higher carbon content. A similar trend is found in Fig. 3, where peak broadening increases with lower deposition temperatures. Two common methods of estimating grain sizes from XRD are the Scherrer equation, which treats line broadening purely as an effect of particle size, and the Williamson-Hall method, which also incorporates intrinsic strain as a source

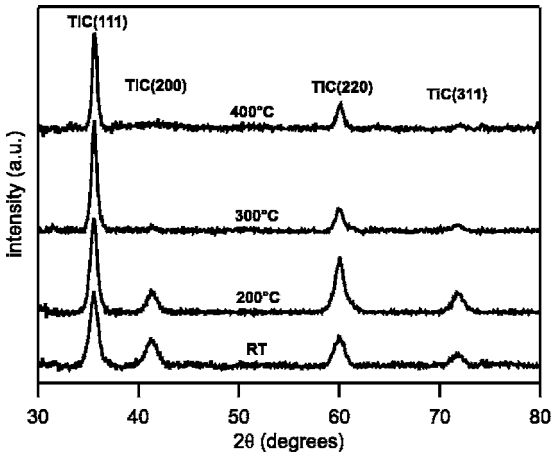

FIG. 3. Diffractograms from GI scans for samples deposited at different temperatures. All samples have carbon contents of 51–55 at. % and are deposited on Al_2O_3 substrates.

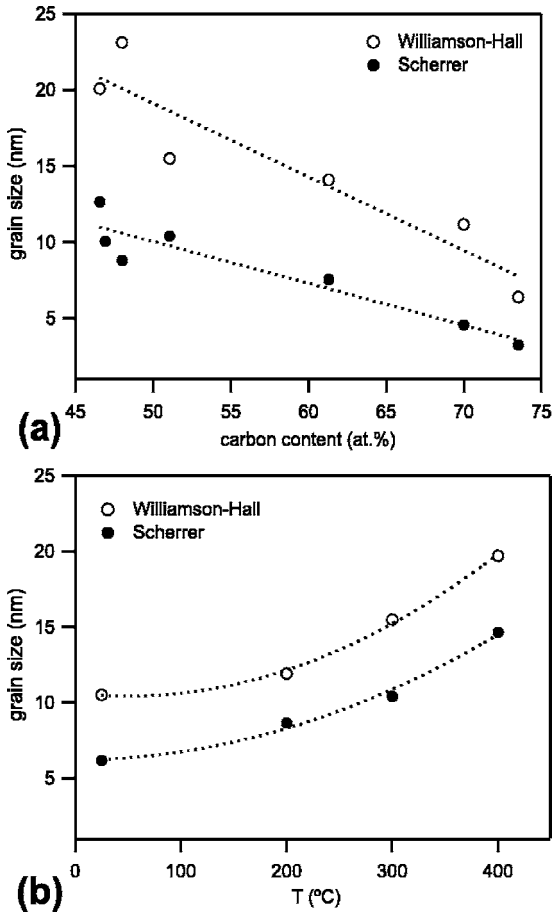

FIG. 4. Span for probable TiC_x-crystallite sizes (a) as a function of total carbon content in films deposited at 300 °C and (b) as a function of deposition temperature for samples with carbon contents of 51–55 at. %. Open circles are calculated with the Williamson-Hall method and solid circles with the Scherrer equation. Lines are only intended as guides for the eyes.

of line broadening.[22–24] In Fig. 4 ranges of probable crystallite size for samples with different carbon contents (a) and deposited at different temperatures (b) are presented. We have used the Scherrer equation as the lower limit, and the Williamson-Hall method as the upper limit of this span. The difference in the estimated grain size between the Scherrer and the Williamson-Hall methods implies that there are intrinsic stresses present in the nc-TiC_x phase. As can be seen the observed grain size decreases with increased total carbon content and increases with deposition temperature. Due to the uncertain nature of these methods[24] no quantative analysis is attempted, although it is noted that the results indicate a nanocrystalline material with a grain size in the order of a few nanometers to tens of nanometer.

Raman

By using Raman spectroscopy amorphous carbon can easily be identified and to some extent also characterized.[7,15,25] The interesting spectral region for Raman using visible light is between 800 and 2000 cm^{-1}. In this region the so-called *D* and *G* bands caused by sp^2-bonded carbon are visible. The spectral features are directly dependent on the configuration of the sp^2-bonded carbon, which is linked to the amount of sp^2- and sp^3-bonded carbon.[25] In Fig. 5 rep-

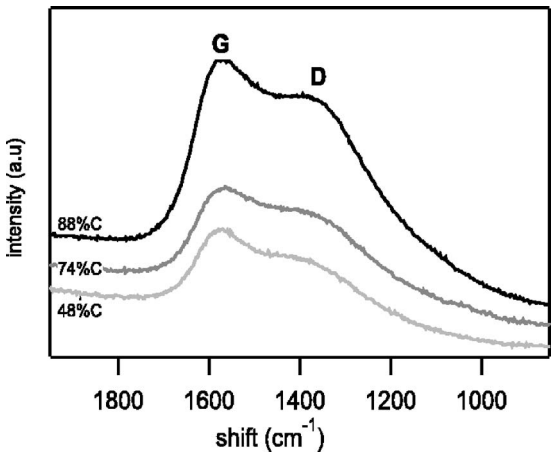

FIG. 5. Typical Raman spectra for nanocomposites containing *a*-C. Spectra for three nc-TiC_x/*a*-C samples with different carbon contents are shown. Spectra recorded with an excitation wavelength of 514 nm.

resentative Raman spectra for three samples with different carbon contents are shown. These spectra exhibit the characteristic mixture of a very broad the *D* band and a somewhat higher *G* band found for amorphous carbon with a high sp^2/sp^3 ratio.[7,25] Such a matrix is expected from literature, where studies on similar coatings deposited by magnetron sputtering have reported amorphous carbon matrices with a high sp^2/sp^3 ratio.[7,15,25] It is hence concluded that, besides the nc-TiC_x phase detected in XRD, also an amorphous, graphitelike carbon phase (*a*-C) exists in the samples.

XPS

XPS analysis enables us to deduce the relative elemental composition of the films and to study the bonding of each element. An investigation of the C1*s* peak [see Fig. 6(a)] shows three peaks, with relative intensities that vary with composition [see Fig. 6(b)]. This leads us to the conclusion that carbon exists in three different chemical surroundings. The two main peaks at about 284.5 and 282 eV are readily identified as C–C and C–Ti bonds, respectively.[7,15,17,26,27] These two peaks are hence clearly associated with the *a*-C and nc-TiC_x phases previously observed in Raman and XRD, respectively. The smaller peak at about 283 eV (marked as TiC^* in Fig. 6) has been reported earlier, although its origin is disputed. It has been suggested that TiC^* represents a separate phase[8,28–30] or may be some sort of interstitial carbon in the TiC phase.[27] It should although be noted that one possibility is that TiC^* is a sputter induced feature due to damaged TiC phase,[30] but indication of a TiC^* peak in unsputtered samples suggests that this is an unlikely explanation.[31]

By comparing the areas of the different subpeaks of the C1*s* spectra (C–C, TiC^*, and C–Ti) the relative amounts of the different carbon-containing phases (*a*-C, TiC^*, and TiC_x) are attained. This is summarized for samples with different carbon contents and for samples deposited at different temperatures in Figs. 7(a) and 7(b), respectively. Furthermore, XPS analysis shows a low oxygen content in the films, which is mainly concentrated in the region close to the surface. Bulk measurements give O concentrations near or below the

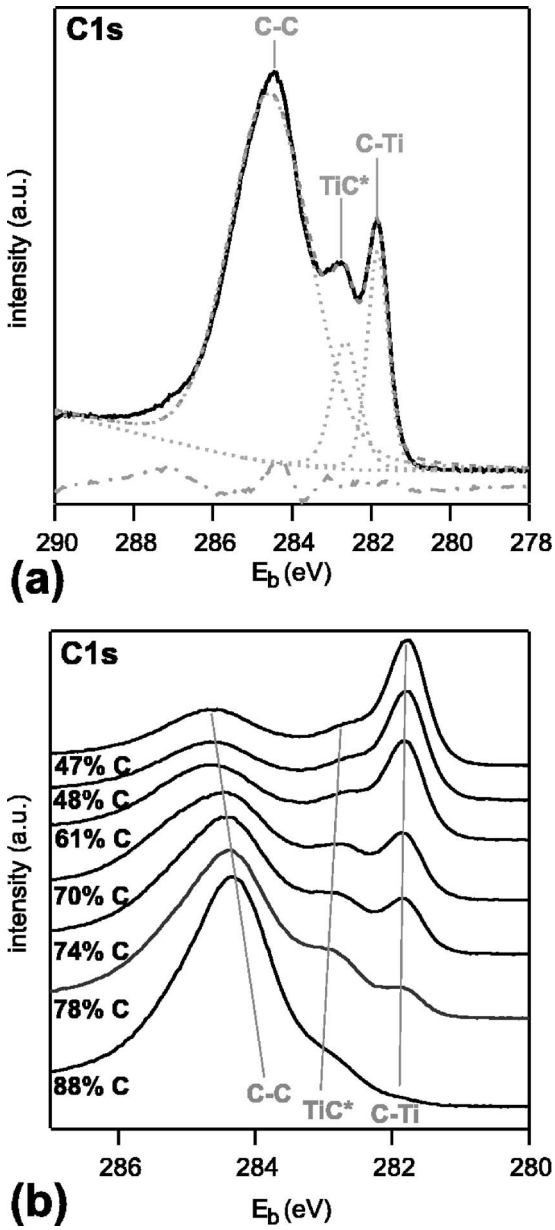

FIG. 6. XPS spectra of the C1*s* peak. (a) The deconvolution for the 70 at. % C sample and (b) for samples with different carbon contents. Three peaks are identified, coming from the *a*-C phase (C–C), the nc-TiC_x phase (C–Ti), and from an interface phase (TiC^*) between the two other phases.

detection limit of XPS. As can be seen from Fig. 6(b) the XPS peaks marked C–C and TiC^* shifts as a function of total carbon content. The C–C peak is shifted from 284.9 to 284.6 eV and the TiC^* peak is shifted slightly from 282.6 to 282.8 eV. These shifts are quite small and present their cause and relevance is unclear.

Properties of nc-TiC/*a*-C films

Electrical properties

The electrical resistivity as a function of composition and deposition temperature is shown in Figs. 8(a) and 8(b), respectively. The variation in resistivity is quite large, and in general the resistivity of the samples ranges from 1200 to 2600 $\mu\Omega$ cm.

The contact resistance, the electrical property that is of importance for the design of coatings for electrical contacts, is in the simplest models proportional to the resistivity of the coating material. However, since many other factors also may play a role, it is important to measure the contact resistance separately.[1–4] In Fig. 9 a typical measurement of contact resistance as a function of contact force is shown for a nc-TiC_x/*a*-C coating and a Ag reference contact (generally considered to be the contact with lowest contact resistance).[32] Depending on film composition and microstructure contact resistances vary; at a contact force of 100 N the contact resistance for our samples varies between 53 and 362 $\mu\Omega$. AFM and SEM investigations of the surfaces pre- and postmeasurements of contact resistance show that the coatings are intact after testing. Observed roughness values (R_a, rms, and total z range) for all samples are all within the variations of blank substrates, both before and after testing.

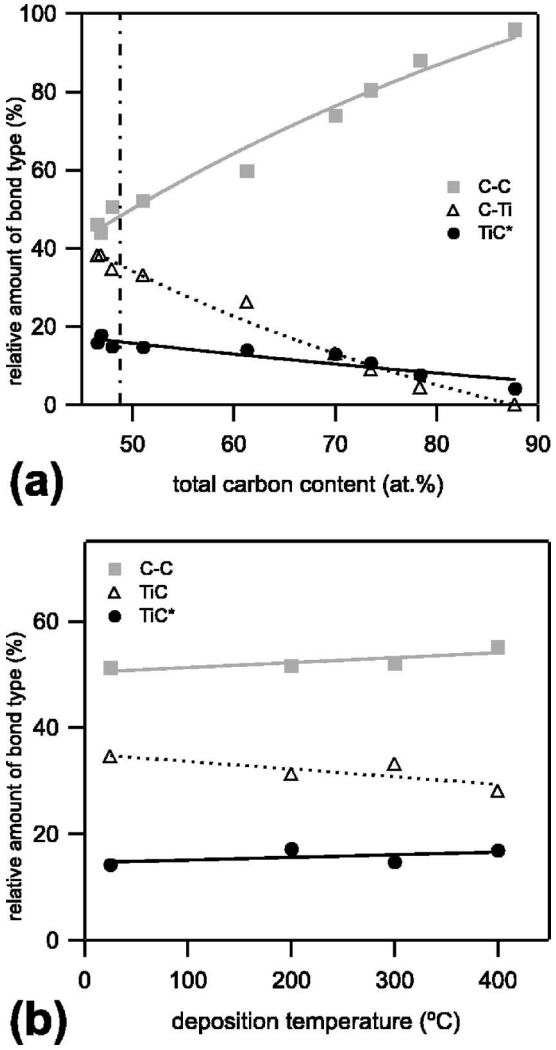

FIG. 7. The relative amount of the different bond types, as found by deconvolution of C1*s* XPS spectra, (a) as a function of total carbon content for samples deposted at 300 °C and (b) as a function of deposition temperature for samples with carbon contents of 51–55 at. %. The dash-dotted line represents the upper limit of the stability region for TiC_x; other lines are only intended as guides for the eyes.

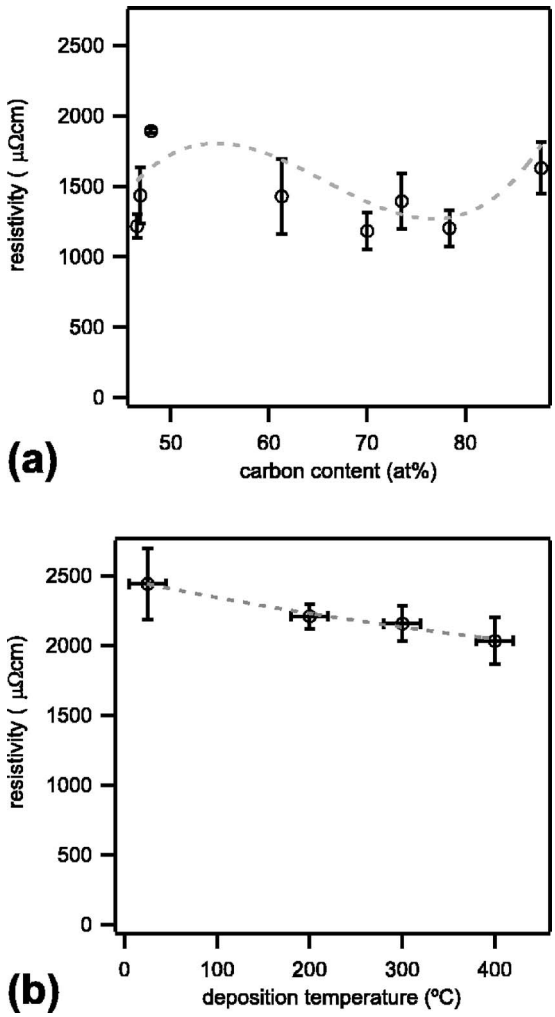

FIG. 8. The electrical resistivity as a function of (a) film composition, where all shown samples were deposited at 300 °C, and (b) deposition temperature, where samples have carbon contents of 51–55 at. %. Lines are only intended as guides for the eyes.

Mechanical properties

Since the mechanical the properties of thin films in the nc-TiC/*a*-C system have been intensely studied elsewhere,[7,8,15–18] measurements were only made on two samples to confirm that the deposited films have expected hardness and elastic modulus. The investigated samples were deposited simultaneously on different substrates and have a carbon content of 55 at.%. The attained load and unload curves from nanoindentation are shown in Fig. 10. The film deposited on the polished steel substrate shows both higher hardness and elastic modulus (12 and 171 GPa, respectively) than the film deposited on the contact substrate (9 and 120 GPa, respectively), which has a higher surface roughness. This clearly shows the importance of the substrate material. Something, however, which is quite similar, is the elastic recovery, which unfortunately cannot be fully evaluated due to the lack of measuring points in the unload curve. The calculated values are in good agreement with those found in literature, possibly our values are somewhat lower than reported elsewhere for nc-TiC/*a*-C.[5,7,33] In comparison one can note that thin films of pure $TiC_{0.8}$ has a hardness of 30 GPa and an elastic modulus of 388 GPa,[34] and that the

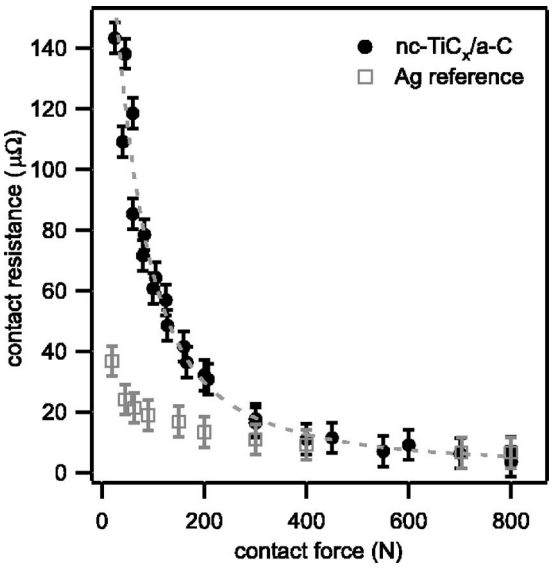

FIG. 9. Contact resistances as a function of contact force. Representative sample deposited at 400 °C with a carbon content of 48 at. % (filled circles) and Ag reference sample (open squares). All measurements were made with Ag counter contacts. Line only intended as a guide for the eyes.

hardness of substoichiometric TiC_x is known to increase with x.[35,36] From pin-on-disk measurements the coefficient of friction (μ) against ball-bearing steel was determined to be 0.19. This clearly indicates the low-friction behavior of the films. In comparison it can be mentioned that measuring under the same circumstances steel against steel yields a friction coefficient of 0.7.

DISCUSSION

Phase composition and microstructure

From the results above we conclude that the deposited thin films are nanocomposites of nanocrystalline TiC (nc-TiC) and graphitelike amorphous carbon (a-C). This is in agreement with earlier published work on sputtered Ti–C coatings.[5,7,8,12,33] As can be seen from Fig. 4(b) the grain size can clearly be controlled by deposition temperature. It should

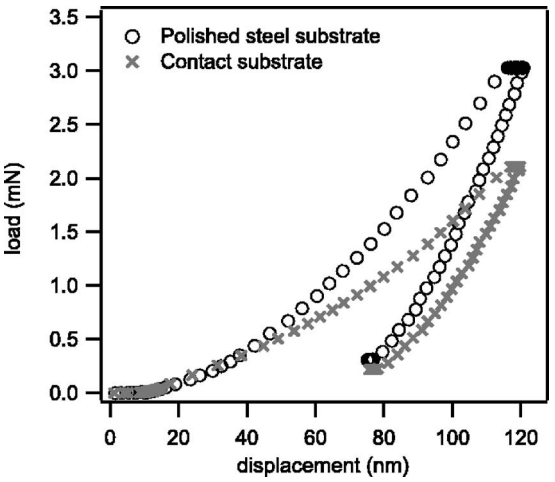

FIG. 10. Load and unload curves from nanoindentation measurements for nc-TiC/a-C nanocomposite thin film deposited on polished steel (circles) and contact (crosses) substrates.

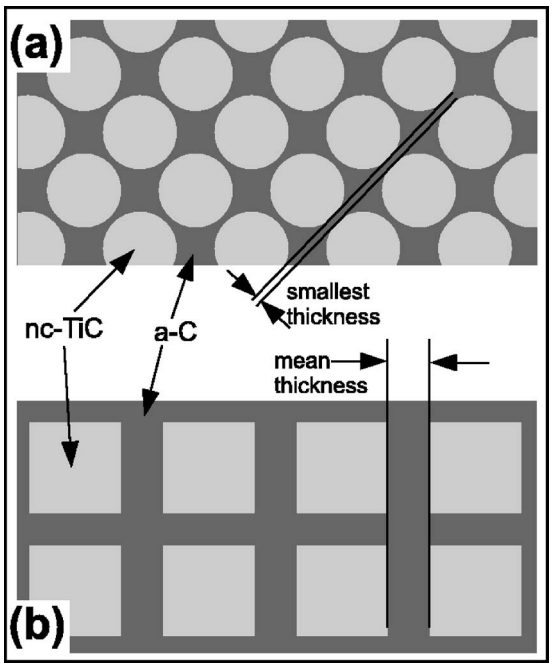

FIG. 11. Sketches of the two models used for estimation of matrix phase thickness. TiC_x grains in light gray and a-C matrix in dark gray.

although be noted that an increased temperature not only influences the grain size (through increased surface mobility during film growth) but may also influence the phase composition.

By using two simple models we have approximated the thickness of the a-C matrix between the TiC_x-grains. Both models are based on the same idea, an "expanded close packing" of particles where the amount of space between the grains depends on amount of matrix phase. We have used approximate grain sizes from XRD measurements (using the Williamson-Hall method, see above) and relative amounts of TiC_x and a-C phases from XPS analysis (see Fig. 7), together with literature values of density and molar weight of respective species. Using these values we can easily calculate the distance between the TiC_x grains (i.e. matrix thickness) that is required to accommodate the observed amount of matrix phase. We have used two model cases: spherical grains, i.e., an expanded fcc lattice of grains with matrix phase in the interstices [Fig. 11(a)] and cubical grains, i.e., stacking of cubes with matrix phase in between the cubes [Fig. 11(b)]. From the former we have approximated a minimal matrix thickness (the shortest distance between the grains coming from the face diagonal of the fcc lattice), and from the latter model we have calculated a mean matrix thickness (the distance between the cubes). The result of the above-described modeling for samples deposited with different carbon contents is presented in Fig. 12. The minimal matrix thickness varies from 0.06 to 2 nm and the mean matrix thickness is between 2 and 3 nm. These result are in the lower end of matrix thickness reported by Voevodin and Zabinski for similar coatings.[7] The differences can at least partly be attributed to different deposition techniques.

From the total composition and the relative amounts of respective phases, the composition of the TiC_x phase can be calculated under the assumption that the assumed TiC^* phase

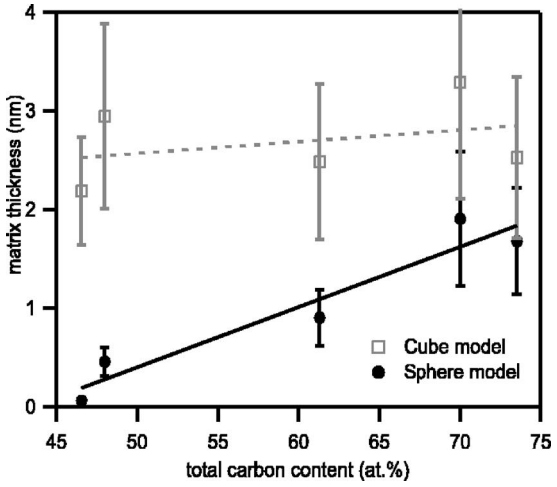

FIG. 12. The mean (open cubes) and minimal (filled circles) matrix thicknesses as a function of total carbon content. Plotted samples vary in composition, but were all deposited at 300 °C. Lines are only intended as guides for the eyes.

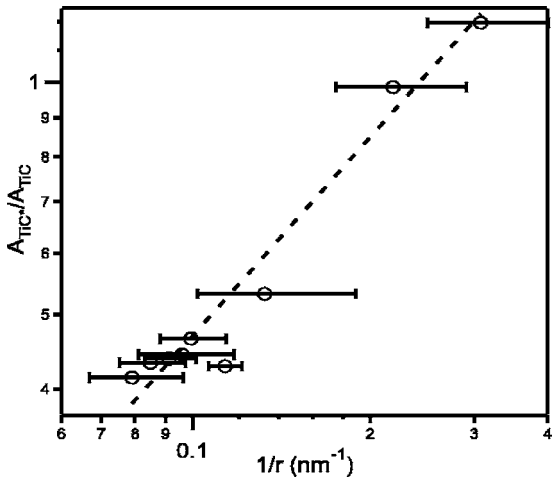

FIG. 14. Ratio of the two phases TiC* and TiC (A_{TiC^*}/A_{TiC}) against the inverted grain size ($1/r$) estimated with the Scherrer equation. The almost linear relation (dashed line) supports the notion that TiC* is an interface phase situated as a surface layer on the TiC-grains. Plotted samples vary in carbon content but were all deposited at 300 °C.

has the same composition. The TiC_x phase is found to be substoichiometric, x varies from 0.44 to 0.64 (see Fig. 13). This is well below the upper limit of 0.95, which represents the upper limit of the thermodynamically stable region for TiC_x at 49 at. % carbons.[21] From a thermodynamical point of view this is not what is expected (for samples with a total carbon content above 49 at. % it should be possible to form ($TiC_{0.95}$), although it is in agreement with what has been reported earlier for magnetron sputtered nc-TiC/a-C films.[17] The low amount of carbon within the TiC_x phase leads to a larger amount of matrix (a-C) phase than otherwise expected. In Fig. 13 an increase of x with higher carbon content can be observed for samples with much Ti. This trend is broken for samples with a carbon content above 65 at. %. A possible reason for this is that 4–8 at. % Ti may be dissolved in the matrix phase,[5] something which has not been taken into account during the calculation of x.

As noted above the origin of the TiC* peak is disputed. We propose that the peak observed in our samples arises from an interface layer between the nc-TiC_x and the a-C matrix, which could have the observed chemical shift. Such an interface layer has been suggested earlier, and it has been proposed that such a layer has good bonding properties and supports high electrical conductivity.[28] In a simple model where a thin layer of TiC* covers each TiC grain the amount of TiC* would be proportional to the surface area of the grain and the amount of TiC would be proportional to the volume of the grain. For a spherical grain this means that the amount of TiC* would be proportional to r^2 (r being the grain size) and the amount of TiC would be proportional to r^3. Hence the ratio of TiC*/TiC (experimentally found through the area of respective sub peaks observed in XPS) would be proportional to $r^2/r^3 = 1/r$. In Fig. 14 a plot of the ratio between the areas from respective subpeaks (A_{TiC^*}/A_{TiC}) against $1/r$ is shown for samples with different carbon contents, all deposited at 300 °C. The almost linear relation is taken as a strong indication that TiC* represents an interface phase between the TiC_x grains and a-C matrix.

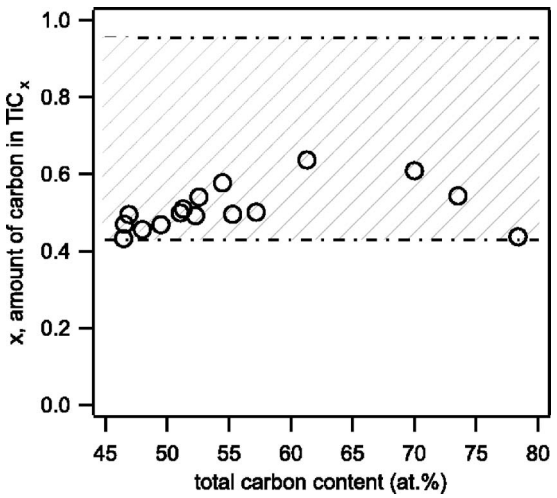

FIG. 13. Carbon content in TiC_x phase, x as a function of total carbon content. The area between the dash-dotted lines represents the stability region for TiC_x.

In Fig. 7(b) the relative amounts of phases for samples deposited at different temperatures are shown. As can be seen no clear trends exist. Since we have observed above an increased grain size with increased temperature, this lack of trends is in contrast with our hypothesis that TiC* is an interface phase in between the TiC_x crystallites and the a-C matrix; a decreased relative amount of TiC* should be observed for samples deposited at high temperatures. However, deposition temperature may also influence the phase composition. To determine the nature of the TiC*-phase studies where grain size is varied independent of the total composition and deposition temperature is required.

From the analysis of the films we hence conclude that our samples are nanocomposites of nanometer-sized substoichiometric TiC_x crystallites (nc-TiC_x) embedded in an amorphous matrix of mostly graphitelike carbon (a-C). The size of the crystallites (for our samples in the order of a few to tens of nanometer) can be controlled through deposition temperature, although this deposition parameter also may in-

fluence the phase composition. The relative amount of nc-TiC_x (4–40 at. %) and *a*-C (44–96 at. %) phases can be controlled by the total carbon content (i.e., the current or effect setting of the magnetrons during deposition). The increase of the relative amount of *a*-C phase has in our experiments been coupled to a decrease in grain size. By combining temperature control and control over the phase composition one should (within reasonable limits) be able to deposit films with a desired grain size and desired amount of matrix phase, hence controlling the matrix thickness (mean thickness in our samples is 1.3–3.3 nm). The third phase, TiC^*, is probably an interface phase situated between the nc-TiC_x grains and the *a*-C matrix, and its relative amount is closely related to grain size and possibly deposition temperature.

Properties

The observed resistivity (1200–2600 $\mu\Omega$ cm) is significantly lower than the value of a sample of pure sputtered *a*-C, which has a resistivity of 38 000 $\mu\Omega$ cm, and significantly higher than what has been reported for other similar thin film systems. Due to the large amounts of microstructural parameters that may influence the resistivity in these types of films one cannot expect to have the same values as other published results from samples deposited through similar techniques. Still comparisons can be interesting to find possibilities for improved performance. Gulbinski *et al.*[17] have published results where nc-TiC/*a*-C:H films have resistivities ranging from 75 to 700 $\mu\Omega$ cm in comparable composition ranges. The low values are probably due to that small amounts of Ti metal that coexist in their material and hence lowering the resistivity.[37] Pure TiC samples deposited by Santerre *et al.*[38] gave resistivities of 80–140 $\mu\Omega$ cm. One factor of great importance for the resistivity is the composition of the TiC_x phase, a substoichiometric TiC_x will due to carbon vacancies (point defects) have a higher resistivity.[39] Since the TiC_x phase can be the phase expected to contribute the most to the electrical conduction, this may be a part of the explanation of the high observed values for our coatings. The samples deposited at different temperatures show a slight decrease in resistivity as deposition temperature is increased [see Fig. 8(b)]. A plausible explanation for this is that the increased grain size gives fewer grain boundaries (i.e., scattering points) per length scale, hence lowering the resistivity. For samples deposited with different compositions no trends with respect to microstructural or depositional parameters can be identified. The reason for this is probably that several microstructural parameters are changed simultaneously in these samples, and hence making the analysis difficult. Further studies where microstructural parameters are separated are required. Interesting for later comparison of contact resistance measurements are films deposited by Eklund *et al.*,[14] where nc-TiC is embedded in an amorphous matrix of SiC (*a*-SiC). These films have showed resistivities of 250–1160 $\mu\Omega$ cm.

As can be seen from Fig. 9 the observed contact resistance of the nc-TiC_x/*a*-C coating is in the same order of magnitude as the Ag reference. This clearly indicates that this type of nanocomposite material is a good candidate for contact coatings. Furthermore one should notice that it matches more or less the performance of more or nc-TiC_x/*a*-SiC coatings deposited by Eklund *et al.*, which has a contact resistance of 37 $\mu\Omega$ at a contact force of 100 N for samples deposited on similar substrates.[14] The latter is interesting since the resistivity of our nc-TiC_x/*a*-C coatings is three to five times higher than the nc-TiC_x/*a*-SiC coatings. This means that other factors than resistivity are crucial for the performance of this type of nanocomposites. To be able to understand this we have sought after correlations between microstructural parameters and the contact resistance, which may enable us to optimize and understand the performance of the coatings.

For the series that was varied in total composition there are mainly two microstructural parameters that vary: the amount of matrix phase and the grain size. Both these parameters may influence the contact performance of the coating. Since the matrix phase (*a*-C) is the less conductive phase of the nanocomposite, an increase in this phase is expected to increase the resistivity and contact resistance. On the other hand an increase in matrix phase makes the coating softer, giving a larger area of true contact. One microstructural parameter that indicates the amount of matrix phase in a way that is relevant for an electrical current in the composite is the smallest matrix thickness. Unsurprisingly a plot of the contact resistance against shortest matrix thickness [see Fig. 15(a)] shows that a smaller matrix thickness correlates to a lower contact resistance.

For the samples deposited at different temperatures the main microstructural difference is the grain size. A plot of contact resistance against grain size [see Fig. 15(b)] shows a clear connection between increased grain size and decreased contact resistance. These samples are the same for which the resistivity is shown in Fig. 8(b). The resistivity decreases about 20% but the contact resistance is reduced with about 66%. This despite an increase in smallest matrix thickness. There are hence more factors than just a decrease of resistivity involved here, the nature of which requires more detailed study. What, on the other hand, is clear is that there is space for further optimization of the microstructure. A combination of small matrix thickness and large grain size should yield higher performance. One could argue that this implies that a coating of pure TiC with large grains would be preferable, but such a coating would loose many of the beneficial features of the nanocomposite. Without a soft carbon matrix the coating will be much harder, diminishing the deformation required for good electrical contact and increasing the friction. The friction will also be increased due to the lack of "free" carbon that can form a tribofilm, reducing the friction. Additionally increasing the grain size considerably requires that energy be added to the film during growth by means of radiative heating or energetic particles. This will unavoidably lead to substrate heating. As mentioned above the use of metal substrates in contacts makes substrate heating undesirable. There is probably an optimum for the grain size, at some point the grain size becomes so large that traditional composite mixing rules start to apply and the performance decreases. A study where mechanical properties as well as

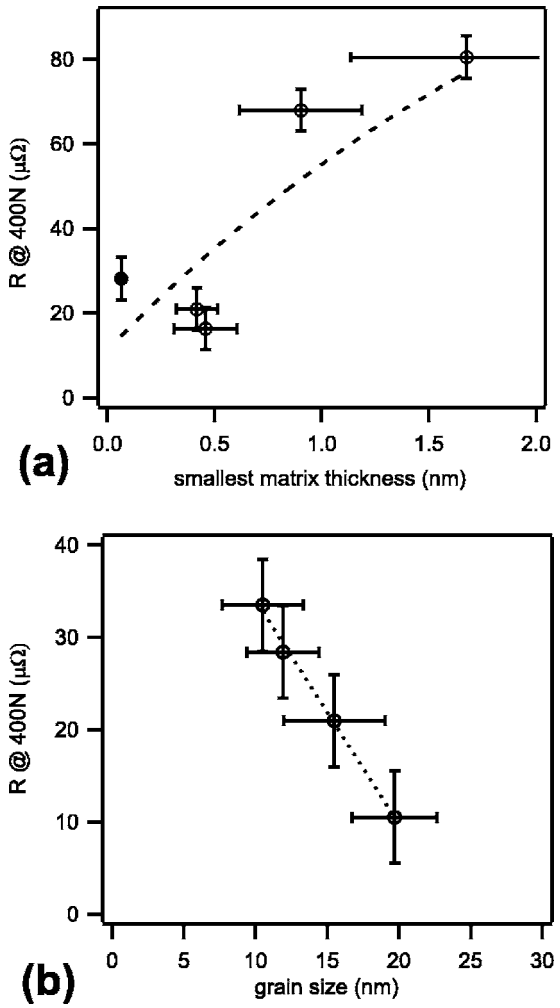

FIG. 15. (a) The contact resistance at a contact force of 400 N as a function of minimum matrix thickness (determined in Fig. 12). Samples deposited at 300 °C and vary in total carbon content. (b) The contact resistance plotted against grain size. Samples deposited between 25 and 400 °C, with total carbon contents of 51–55 at. %. Lines only intended as guides for the eyes.

contact properties are correlated to each other and the microstructure is required to attain understanding of the optimization problem, as well as a study investigating the upper limit of the grain size.

CONCLUDING REMARKS

We have, using nonreactive dc-magnetron sputtering, deposited coatings of nc-TiC_x/*a*-C nanocomposites. These coatings show promising performance as coatings on contact surfaces, with contact resistance comparable to traditional metallic coatings but with clearly superior mechanical properties. This makes nc-TiC_x/*a*-C nanocomposites an interesting candidate as coating material for contacts that are subject to frequent wear and friction (i.e., sliding or switching contact arrangements). The well-known possibility to tailor the mechanical properties of nc-TiC_x/*a*-C nanocomposite thin films coupled with the above indicated possibility to design electrical contact properties through microstructural control makes this material even more interesting for usage as a tailored coating on high-performance contact components. Compared to earlier tailoring of mechanical properties, the frequent use of metals with low melting point in contact applications limits some of the optimization routes since the deposition temperature must be kept low. Before this material can be used in applications further studies on contact specific properties such as fritting, aging, and corrosion resistance are required.

One manner in which contact performance could be increased even further is doping with noncarbide forming metal, which would enhance the electrical conductivity of the matrix phase. We will investigate in future studies this possibility and manners in which individual microstructural parameters (such as matrix thickness) can be controlled independently of other microstructural parameters, so that a better understanding of the properties governing the contact performance can be attained.

ACKNOWLEDGMENTS

The authors wish to acknowledge the financial support of the Swedish Foundation for Strategic Research (SSF) and the Swedish Research Council (VR), as well as the assistance of Impact Coatings, Linköping, Sweden for being able to use their equipment and Mattias Carlsson at the department for Engineering Sciences, Uppsala University, for assistance with measurements of mechanical properties. The authors also wish to thank Peter Isberg and Åke Öberg at ABB Corporate Research, Västerås, Sweden, for assisting in application specific questions.

[1] R. Holm, *Electric Contacts: Theory and Applications*, 4th ed. (Springer-Verlag, Berlin, 2000); 1st ed. (Springer-Verlag, Berlin, 1967).
[2] R. S. Timsit, IEEE Trans. Compon. Packag. Technol. **22**, 85 (1999).
[3] R. S. Timsit, in *Electrical Contacts: Principles and Applications*, edited by P. G. Slade (Dekker, New York, 1999), pp. 1–88.
[4] J. A. Greenwood, Br. J. Appl. Phys. **17**, 1621 (1966).
[5] B. Feng, D. M. Cao, W. J. Meng, J. Xu, R. C. Tittsworth, L. E. Rehn, P. M. Valdo, and G. L. Doll, Surf. Coat. Technol. **148**, 153 (2001).
[6] W. Wu and J. Ting, Thin Solid Films **420/421**, 166 (2002).
[7] A. A. Voevodin and J. S. Zabinski, J. Mater. Sci. **33**, 319 (1998).
[8] M. Stüber, H. Leiste, S. Ulrich, H. Holleck, and D. Schild, Surf. Coat. Technol. **150**, 218 (2002).
[9] D. Nilsson, F. Svahn, U. Wiklund, and S. Högmark, Wear **254**, 1084 (2003).
[10] C. Benndorf, E. Boettiger, M. Fryda, H. G. Haubold, C.-P. Klages, and H. Körbele, Synth. Met. **41–43**, 4055 (1991).
[11] A. Grill, Thin Solid Films **355/356**, 189 (1999).
[12] D. Martinez-Martinez, C. Lopez-Cartes, A. Justo, A. Garcia-Luis, M. Brizuela, and J. I. Onate, J. Vac. Sci. Technol. A **23**, 1732 (2005).
[13] Y. T. Pei, D. Galvan, J. T. M. DeHosson, and A. Cavalerio, Surf. Coat. Technol. **198**, 44 (2005).
[14] P. Eklund *et al.*, J. Vac. Sci. Technol. B **23**, 2486 (2005).
[15] S. Zahng, X. L. Bui, J. Jiang, and X. Li, Surf. Coat. Technol. **198**, 206 (2005).
[16] A. A. Voevodin, S. V. Prasad, and J. S. Zabinski, J. Appl. Phys. **82**, 855 (1997).
[17] W. Gulbinski, S. Mathur, H. Shen, T. Suszko, A. Gilewicz, and B. Warcholinski, Appl. Surf. Sci. **239**, 302 (2005).
[18] T. Zehnder and J. Patscheider, Surf. Coat. Technol. **133/134**, 134 (2000).
[19] W. C. Oliver and G. M. Pharr, J. Mater. Res. **7**, 1564 (1992).
[20] M. C. Morris, H. F. McMurdie, E. H. Evans, B. Paretzkin, H. Parker, N. P. Pyrros, and C. R. Hubbard, NBS Monogr. **25**(18), 73 (1981).
[21] J. L. Murray, *Phase Diagrams of Binary Titanium Alloys* (ASM International, Metals Park, OH, 1989).
[22] B. D. Cullity, *Elements of X-Ray Diffraction*, 2nd ed. (Addison-Wesley Reading, MA, 1978).
[23] G. K. Williamson and W. H. Hall, Acta Metall. **1**, 22 (1953).
[24] P. Scardi, M. Leoni, and R. Delhez, J. Appl. Crystallogr. **37**, 381 (2004).
[25] A. C. Ferrari, New Diamond Front. Carbon Technol. **14**, 87 (2004).

[26]*Handbook of X-Ray Photoelectron Spectroscopy*, edited by G. R. Muilenberg (Perkin-Elmer Corporation, Physical Electronics Division, Eden Prairie, 1979).
[27]G. Li and L. F. Xia, Thin Solid Films **396**, 16 (2001).
[28]V. Schrier, H.-J. Michel, and J. Halbritter, Fresenius' J. Anal. Chem. **346**, 227 (1993).
[29]B. Hornetz, H.-J. Michel, and J. Halbritter, Fresenius' J. Anal. Chem. **349**, 233 (1994).
[30]A. Mani, P. Aubert, F. Mercier, H. Khodja, C. Berthier, and P. Houdy, Surf. Coat. Technol. **194**, 190 (2005).
[31]J. Luthin, H. Planck, J. Roth, and C. Linsmeier, Nucl. Instrum. Methods Phys. Res. B **182**, 218 (2001).
[32]W. Rieder, *Electrical Contacts: An Introduction to Their Physics and Applications* (IEEE, New York, 2005).
[33]S. Zhang, X. L. Bui, J. Jiang, and X. Li, Surf. Coat. Technol. **198**, 206 (2005).
[34]H. Högberg, J. Birch, M. Odén, J.-O. Malm, L. Hultman, and U. Jansson, J. Mater. Res. **16**, 1301 (2001).
[35]J.-L. Chermant, P. Delavignette, and A. Deschanvres, J. Less-Common Met. **21**, 89 (1970).
[36]M. Guemmaz, A. Mosser, L. Boudoukha, J. J. Grob, D. Raiser, and J. C. Sens, Nucl. Instrum. Methods Phys. Res. B **111**, 263 (1996).
[37]S. Mathur (private communication).
[38]F. Santerre, M. A. ElKhakani, M. Ckaker, and J. P. Dodelet, Appl. Surf. Sci. **148**, 24 (1999).
[39]W. S. Williams, Mater. Sci. Eng., A **105/106**, 1 (1988).